ORIGINAL ARTICLES

Shape Changes in the Cleft Palate Maxilla: A Longitudinal Study

PETE E. LESTREL, PH.D.
SAMUEL BERKOWITZ, D.D.S., M.S., F.I.C.D.
OSAMU TAKAHASHI, D.D.S., D.D.SC.

Objective: **The purpose of this study was to compare the shape of the maxilla in *Norma lateralis* of cleft lip and palate (CLP) patients with non-CLP controls matched for sex and age. This study utilized elliptical Fourier functions to assess the presence of residual shape changes in the cleft palate maxilla after treatment, compared with controls.**

Design: **Longitudinal data (n = 25) were available from the Miami Craniofacial Anomalies Foundation. From these data, two samples were selected: group I (mean age and SD, 5.06 ± 1.82 years) after lip surgery and the initiation of palate surgery and group II (16.58 ± 2.42 years) well after the conclusion of surgery. Twenty-two of these patients were matched with controls (5.11 ± 1.33 and 15.91 ± 2.25 years, respectively). The maxillary outline as seen on the lateral radiograph was (1) traced, (2) fitted with a series of 48 closely placed points, (3) digitized, and (4) submitted to a specially written routine that computes elliptical Fourier functions (EFFs). These EFFs are close analogs of the bounded maxillary outline as judged by the residual or difference between the observed points and the predicted points generated by the Fourier function. Each maxillary outline was subsequently standardized for size and corrected for positioning in two-dimensional space.**

Results and Conclusions: **Utilizing a three-way multivariate analysis of variance, statistically significant shape differences were obtained for both young and older groups, as well as between the CLP and controls. No significant gender differences were found. Morphological differences consisted of a posterior repositioning of the nasal crest aspect in the CLP cases. These results suggest that although a clinically satisfactory treatment result was obtained, differences in maxillary shape remain.**

KEY WORDS: *cleft palate, elliptical Fourier functions, growth, maxilla, shape*

Cleft palate and its associated syndromes comprise one of the more common congenital abnormalities in the craniofacial complex. In spite of considerable research, the causal mechanisms responsible for cleft lip and palate (CLP) are not fully understood. Surgical procedures, however, have been steadily improving, with the consequence that most patients today generally present an acceptable treatment result. The primary aim of orthognathic surgery, orthopedics, and orthodontics in the management of CLP is the correction of these maxillofacial malformations so that the treatment outcome is as close to normal as possible. The treatment goals are not only improving facial esthetics, but they are also creating a palate that is functioning adequately with respect to swallowing, mastication, and speech.

Dr. Lestrel is in the Section of Oral Biology, University of California-Los Angeles School of Dentistry, Los Angeles, California. Dr. Berkowitz is at the University of Miami School of Medicine, Miami, Florida. Dr. Takahashi is in the Department of Orthodontics, Nihon University School of Dentistry at Matsudo, Chiba, Japan.

Presented in part at the 76th Annual Meeting of the International Association for Dental Research, June 24–27, 1998, Nice, France.

Submitted June 1998; Accepted December 1998.

Reprint requests: Dr. Pete E. Lestrel, 7327 De Celis Place, Van Nuys, CA 91406-2853. E-mail: plestrel@ucla.edu

Cleft Palate Maxillary Growth

While the literature on cleft palate and its associated syndromes is extensive, much of it has focused on changes in the dental occlusion and the effect of treatment on the facial profile. The sizes of the dental arches in CLP cases tend to be smaller than normal (Jonsson and Thilander, 1976), and palatal height has also been reported to be less on the cleft side (Mølsted and Dahl, 1990). A study of unoperated complete bilateral CLP patients demonstrated that the dental arch widths were greater when compared to controls (Bishara et al., 1985). Another serial cast study of bilateral CLP patients showed that the maxillary arch depth (vault height), while equivalent to controls from 6 to 10 years of age, decreased significantly from 11 to 17 years of age, compared to controls (Heidbuchel and

Kuijpers-Jagtman, 1997). Lateral cephalometric data also suggest that the CLP cases display smaller anatomic measurements compared to those in non-CLP controls (Kilpeläinen et al., 1996). The cleft palate orthodontic literature is replete with descriptive measurement studies reflecting two-dimensional serial changes in palatal and facial size. Berkowitz initially improved on these measuring techniques with the use of stereophotogrammetry and more recently, with the use of three-dimensional digitizing to more adequately describe palatal growth changes (Berkowitz and Pruzansky, 1968; Berkowitz, 1971; Berkowitz et al., 1974; Berkowitz, 1997). All of these studies have focused on the skeletal deficiency and/or the impaired growth of the palatal segments. However, little research is available on how the shape of the CLP maxillary process changes under the influences of growth and the various treatment modalities. Thus, there is a need for geometric growth studies that focus on the form of the CLP maxilla, viewed in global terms (i.e., as a total unit), to document changes in shape, in contrast to size.

Theoretical Considerations

This research focuses on the question of whether the CLP maxilla, as seen on a lateral cephalometric radiograph, exhibits some residual shape changes after treatment. Put somewhat differently, the question raised is, how closely does the CLP maxilla, viewed in global terms, resemble untreated controls—the treatment goal? Ideally, to be clinically beneficial, such presumed differences between CLP cases and controls should be readily apparent visually as well as statistically significant.

Unfortunately, an unambiguous answer to the above question is more difficult to ascertain than may have been realized. The conventional metrical approach (CMA), composed of distances, angles, and ratios, is of limited use because the maxilla shares, with other craniofacial structures, irregularity in form. CMA was originally developed for the measurement of regular geometric objects. It was never intended for the numerical description of complex irregular forms of the type encountered in biology (Lestrel, 1989a, 1997b). Thus, what is required is a procedure that allows for (1) a precise numerical description of the total or global outline of the form, (2) an identification of those localized shape changes that may be significant, and (3) the separation of the confounding factor of size from shape.

During the last two decades, a variety of new and mathematically sophisticated methods to deal with the limitations of the CMA have been generated. These various methods can be subsumed under two broad approaches, which have been categorized as homologous-point– or landmark-dependent– and boundary-outline–based procedures (Read and Lestrel, 1986; Lestrel, 1989a; Read, 1990).

The former includes conventional metrics as well as newer methods, such as finite elements (Cheverud and Richtsmeier, 1986; Richtsmeier, 1988), biorthogonal grids (Bookstein, 1978, 1982), thin-plate splines (Bookstein, 1991), and Euclidean distance matrix analysis (EDMA) (Lele and Richtsmeier, 1991, 1992; Lele, 1993).

The latter includes eigenshape analysis (Lohmann, 1983; Lohmann and Schweitzer, 1990; Ray, 1990), medial axis functions or line skeleton (Blum, 1967, 1973; Straney, 1990), and Fourier descriptors (Lestrel, 1974, 1980, 1982; Johnson, 1985; Delfino et al., 1986; Lestrel, 1989b; Diaz et al., 1990; Inoue, 1990; Lestrel and Kerr, 1993).

While many of the above methods have provided new data and useful information, Fourier descriptors, specifically elliptical Fourier functions (EFFs), are particularly well suited for characterizing the boundary outline of irregular morphologies such as those encountered in the craniofacial complex. EFFs, as utilized here, allow for the numerical description of the boundary outline of the maxilla as seen on a lateral X-ray. EFFs also allow for control for size differences and provide a method by which differences in shape can be identified (Lestrel et al., 1991; Lestrel, 1997a).

Elliptical Fourier Functions

EFFs, a relatively new Fourier descriptor, are related to the conventional Fourier series. This was the method of choice, not only because it is free of some of the limitations of CMA but also because a much larger class of morphological forms can be fitted in contrast to traditional Fourier analysis (Lestrel, 1989a). The EFF was originally developed by Kuhl and Giardina (1982), who used it for military applications to rapidly identify aircraft. It was subsequently used to characterize the shape of mosquito wings for classification purposes (Rohlf and Archie, 1984; Ferson et al., 1985). Recent applications have dealt with the shape of selected bones in the human craniofacial complex (Lestrel, 1989b; Lestrel et al., 1991; Lestrel and Kerr, 1993; Lestrel, 1997a).

The procedure of EFF is a parametric solution. That is, the representation of the points (x, y) on the curve in two dimensions is in the form of a pair of equations written as function of a third variable (t). (This method has been extended to three dimensions (x, y, z) to produce a curve in space (Lestrel, 1997a). However, this is not a volumetric solid, which is precluded by the parametric formulation.) Any two-dimensional outline can be approximated with a polygon by connecting the observed data points with straight lines. Note that the distances between data points can vary. The closer the spacing of the observed points, the more accurate the representation. The projection of these points into either the x- or the y-axis can be defined as a function of t. Because these new functions are piecewise linear, single valued, and periodic, they can also be fitted with Fourier functions (Kuhl and Giardina, 1982). The separate projections (along the x- and y-axes) of the parametric formulation can be visualized as follows. Consider the y-coordinate values being projected or "embedded" into the y-axis and then replotted against a new horizontal "x-axis," which is now labeled the "t-axis." The x coordinate is treated in an identical manner. Once the expected x and y coordinates have been separately computed, one can "rejoin" these coordinates (for identical values of t), and the expected shape can be recreated. If the separate harmonics are plotted, recalling that as

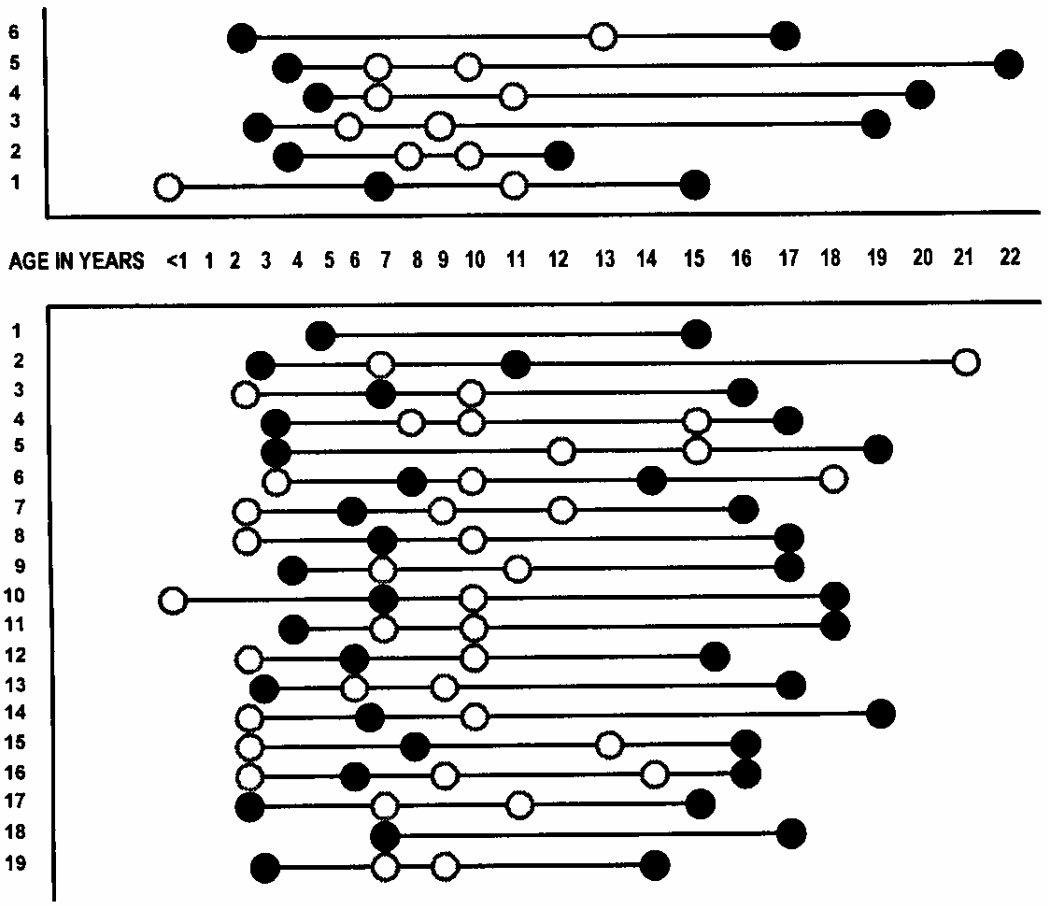

FIGURE 1 Age distributions of the CLP subjects in the study. Closed circles indicate cases that were matched for age and sex with controls.

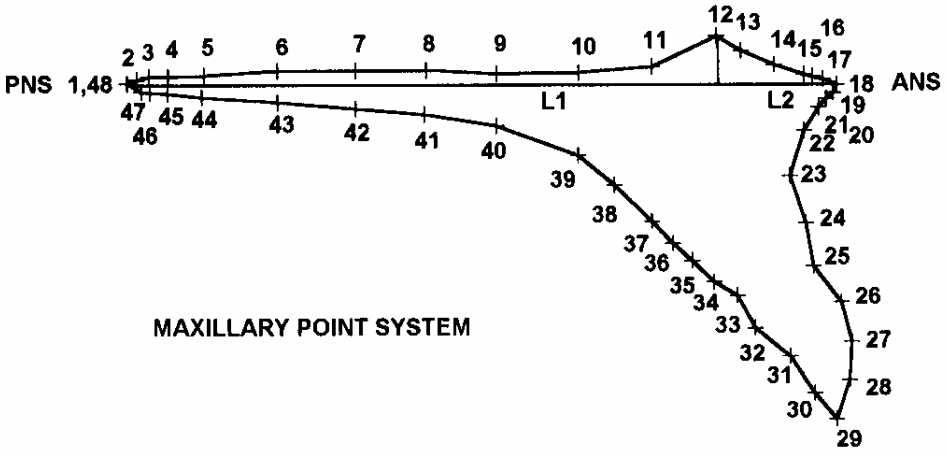

FIGURE 2 The 48-point system used to characterize the maxillary outline. The ANS–PNS line (points 1 and 18) was subdivided into the L1 and L2 segments to facilitate the construction of the additional points on the outline. The tracing was oriented with a horizontal line from ANS to PNS, with PNS placed on at the center (0,0) of the digitizer. The following six anatomical landmarks were initially located and placed on the tracing: point 1 (same as point 48) is PNS; point 12 is the maximum superior extension of the nasal crest; point 18 is ANS; point 25 is the border of the alveolar bone and the anterior incisal margin; point 29 is the tip of the maxillary central upper incisor; and point 33 is the border of the alveolar bone and the posterior incisal margin. See Table 1 for a description of the construction of the remainder of the 48 pseudohomologous points. Note: points 37, 39, 40, 41, 42, 43, and 44 are vertical perpendiculars drawn from points 11, 10, 9, 8, 7, 6, and 5, respectively, using the ANS-PNS line. Asterisks refer to trisections.

TABLE 1 Maxillary Point System*†

Points Defining Line Segments				*Generated Points*			
Above L1	*Above L2*	*ANS (18)–UI TIP (29)*	*UI TIP (29)–PNS (1)*	*L1*	*L2*	*ANS–UI*	*UI–PNS*
1–12	12–18	18–25	29–33	8	14	23	31
1–8	12–14	18–23	29–31	6	13	22	30
1–6	14–18	18–22	31–33	5	15	21	32
6–8	15–18*	18–21*	33–37	7	16, 17	19, 20	35
1–5	—	23–25	33–35	4	—	24	34
1–4	—	25–29	35–37	3	—	27	36
1–3	—	25–27	37–39	2	—	26	38
8–12	—	27–29	44–48	10	—	28	45
8–10	—	—	45–48	9	—	—	46
10–12	—	—	46–48	11	—	—	47

* Points 1(48), 12, 18, 25, 29, and 33 are anatomical landmarks. Points 37, 39, 40, 41, 42, 43, and 44 are vertical perpendiculars drawn from points 11, 10, 9, 8, 7, 6, and 5, respectively, using the ANS–PNS line. Asterisks refer to trisections.

† Construction of the 42-pint system used to characterize the maxillary outline (see Fig. 1). The four columns on the left describe the line segments that were bisected to generate the points shown in the four columns on the right. Line segments identified with asterisks represent trisections—hence, the two points in the two middle right columns.

trigonometric functions they are orthogonal, they produce ellipses. As the terms in the Fourier sequence producing the ellipses are summed (in an identical fashion to the conventional Fourier function), the series will converge onto the polygon that serves as the observed form (see Lestrel, 1997a, for details).

For ease of reference, the parametric equations that define the EFF are shown here. The Fourier series in $x(t)$ is given as:

$$x(t) = A_0 + \sum_{n=1}^{k} a_n\cos(nt) + \sum_{n=1}^{k} b_n\sin(nt) \qquad (1)$$

and the Fourier series in $y(t)$ as:

$$y(t) = C_0 + \sum_{n=1}^{k} c_n\cos(nt) + \sum_{n=1}^{k} d_n\sin(nt). \qquad (2)$$

On this polygon, the first derivative of $x(t)$ or $y(t)$ with respect to t is piecewise constant and can be represented by a Fourier series. This derivative, dx/dt (or dy/dt), consists of a sequence of piecewise-constant terms, $\Delta x_p/\Delta t_p$ (or $\Delta y_p/\Delta t_p$), associated with each division along the polygon (because they are straight lines), t_p to t_{p+1}, over the period T, where $\Delta t_p = (\Delta x_p^2 + \Delta y_p^2)^{1/2}$. Utilizing these properties, Kuhl and Giardina (1982) derived estimates of the elliptical Fourier coefficients that do not require integration, in contrast to conventional Fourier analysis.

Two other aspects require discussion. One of these is the correction for size differences leaving shape differences as a "residual," and the other is the need for a common orientation for superimposition purposes. The area bounded by the observed polygon that serves as the observed form is an appropriate solution to the scaling problem. Size standardization was accomplished by scaling every form, up or down, so that the area was made equal to an arbitrary constant of 10,000 mm^2. Positional orientation of the form in two-dimensional space is accomplished by rotating the form so that the major axis of the first ellipse is made parallel to the x-axis (Kuhl and Giardina, 1982; Lestrel, 1997a). (The more common use of a plane for orientation and superimposition, such as the ANS-PNS line, is not recommended here because the form of the CLP maxilla is abnormal compared to normals. Thus, what is required is a superimposition procedure, which is independent of the class of forms under consideration.) For two-dimensional forms, regardless of their complexity, the EFF is admirably suited as a curve-fitting function.

In sum, the purpose of using EFFs here is that they provide (1) the computation of the bounded area and the centroid (used for superimposition), (2) the ability to control for size differences with a standardization procedure based on area, (3) the attainment of a common orientation in space for superimposition purposes, and (4) the ability to average complex irregular bounded outlines. All four aspects are difficult, if not impossible, to attain with conventional methods.

Materials

Longitudinal cephalometric records of CLP patients were available from the Miami Craniofacial Anomalies Foundation. The data consisted of 25 patients ranging in age from 5 months to 22 years of age. Patients in the treatment group were composed of complete unilateral CLP (♀ = 2, ♂ = 8), incomplete bilateral CLP (♀ = 1, ♂ = 3), and complete bilateral CLP (♀ = 3, ♂ = 8) cases. The mean number of radiographs in each age series was 4.00 ± 0.65. (Note: All values depicted here with a ± refer to the mean and its SD.) The mean age interval between successive radiographic appointments was 4.68 ± 2.34 years. Of the total 99 cephalometric radiographs available, 50 were used in this study (Fig. 1). From these data, two samples were obtained, a young group and an older group, both containing the same individuals: group I (mean age, 5.06 ± 1.82 years), after lip surgery and the initiation of palate surgery, and group II (mean age, 16.58 ± 2.42 years) well after the conclusion of surgery.

A control group was utilized from the Oregon Longitudinal Twin Study collected at the Oregon Health Sciences University in Portland (OR). This control sample was matched for age (mean difference, 0.68 ± 0.96 years) and sex with the CLP cases. Twenty-two cases were available that satisfied the above criteria. Group I consisted of individuals at a young age (5.11 ± 1.33 years), and group II was comprised of the same sub-

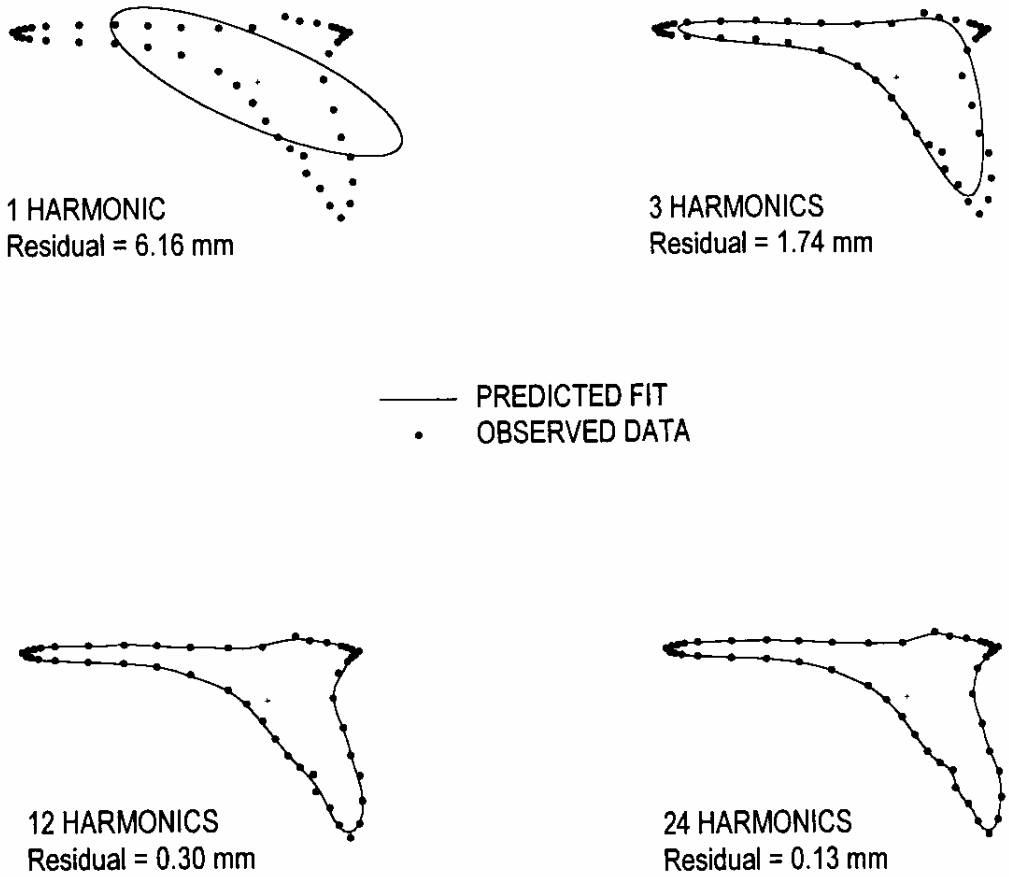

FIGURE 3 Computer-generated stepwise fit to the maxillary outline in two dimensions. The dots represent the observed 48 digitized points. The EFF is shown here as a stepwise process to demonstrate the convergence of the Fourier series to the observed maxillary outline. The first harmonic represents an ellipse. With the addition of three harmonics, the mean residual fit between the expected function and the observed data points was 1.74 mm overall. With 24 harmonics, the mean residual dropped to 0.13 mm for this particular subject.

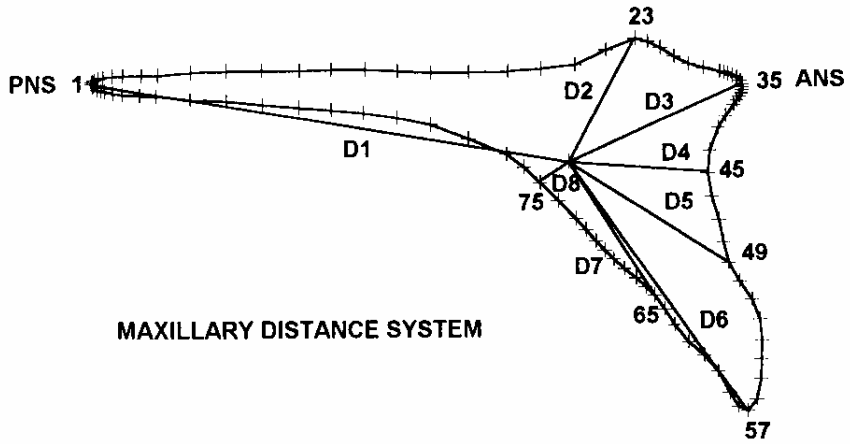

FIGURE 4 The eight distances drawn from the centroid to selected aspects on the maxillary boundary. These eight distances and their *x* and *y* components represent the 24 variables initially used to describe the maxilla. Point numbers are double the original point numbers (Fig. 2) because the EFF curve was constructed with two times the number of data points. This ensured a smoother predicted curve fit.

TABLE 2 Maxillary Distance System*

ID	*Distance from Centroid to*	*Vector Number*
D1	PNS	1
D2	max. superior extension of the nasal crest	23
D3	ANS	35
D4	hard tissue point A	45
D5	alveolar bone border at the anterior incisor margin	49
D6	central incisor tip	57
D7	alveolar bone border at the posterior incisor margin	65
D8	minimum distance of inferior border to centroid	75

* The eight distances drawn from the centroid to selected aspects on the maxillary boundary. These eight distances and their x and y components represent the 24 variables initially used to describe the maxilla. Point numbers are double the original point numbers (Fig. 2) because the EFF curve was constructed with two times the number of data points. This ensured a smoother predicted curve fit (see text).

jects at an older age (15.91 ± 2.25 years). These 22 subjects were then randomly matched with 22 of the CLP patients. Only one twin of each pair was utilized in this study.

Methods

Tracing Procedures

Each maxillary outline as seen on the lateral radiograph was carefully traced onto matte acetate sheets (Herculine drafting film, Keuffel and Esser, Rockaway, NJ) with the use of a 0.3-mm mechanical lead pencil. The outline was drawn from posterior nasal spine (PNS) along the superior palatal surface to anterior nasal spine (ANS), continuing inferiorly to the central incisor tip and back to PNS along the inferior palatal process, resulting in a closed outline (Fig. 2).

Point Locations

The boundary outline of each maxilla was then fitted with a series of 48 closely placed points using an established protocol (Lestrel and Kerr, 1993). Figure 2 displays the six maxillary landmarks and the 42 additional points. The following six anatomical landmarks were initially located and placed on the tracing: (1) point 1 (same as point 48) is the PNS; (2) point 12 is the maximum superior extension of the nasal crest; (3) point 18 is the ANS; (4) point 25 is border of the alveolar bone and the anterior incisal margin; (5) point 29 is the tip of the maxillary central upper incisor; and (6) point 33 is the border of the alveolar bone and the posterior incisal margin.

The other 42 points were then located. A perpendicular was dropped from point 12 to the ANS–PNS line. The distance from PNS to point 10 was labeled L1 and divided into eight equal divisions (Fig. 2). These eight divisions were then extended vertically in a superior direction until they intersected the maxillary outline. These divisions identified seven points 5 to 11. Using these seven points, and counting from PNS, lines were also extended inferiorly until they intersected the maxillary outline. These extensions located the seven points 37 and 39 through 44. Point 4 is the bisection of the distance from point 1 to 5. Point 3 is the bisection of the distance from point 1 to 4. Point 2 is the bisection of the distance from point 1 to 3. Point 45 is the bisection of the distance from point 1 to 44. Point 46 is the bisection of the distance from point 1 to 45. Point 47 is the bisection of the distance from point 1 to 46. Point 38 is the bisection of points 37 and 39. Point 35 is the bisection of points 33 and 37. Point 34 is the bisection of points 33 and 35. Point 36 is the bisection of points 35 and 37. Point 31 is the bisection of points 29 and 33. Point 30 is the bisection of points 29 and 31. Point 32 is the bisection of the distance from point 31 to 33 (Table 1).

The anterior aspect of the maxilla was defined in a similar fashion. The distance from point 12 to ANS was labeled as L2 and divided into four equal divisions. The vertical extensions, in a superior direction, defined points 13 to 15. Points 16 and 17 are trisections of the distance between points 15 and 18. Point 23 is the bisection of the distance from point 18 to 25. Point 22 is the bisection of the distance from point 23 to 18. Point 21 is the bisection of the distance from point 22 to 18. Points 19 and 20 are trisections between points 18 and 21. Point 24 is the bisection of the distance from point 23 to 25. Point 27 is the bisection of the distance from point 26 to 29. Point 26 is the bisection of the distance from point 25 to 27. Point 28 is the bisection of the distance from point 27 to 29. Table 1 is a summary of these point constructions. The four columns on the left represent the points that determined the line segments that were bisected or trisected, while the four

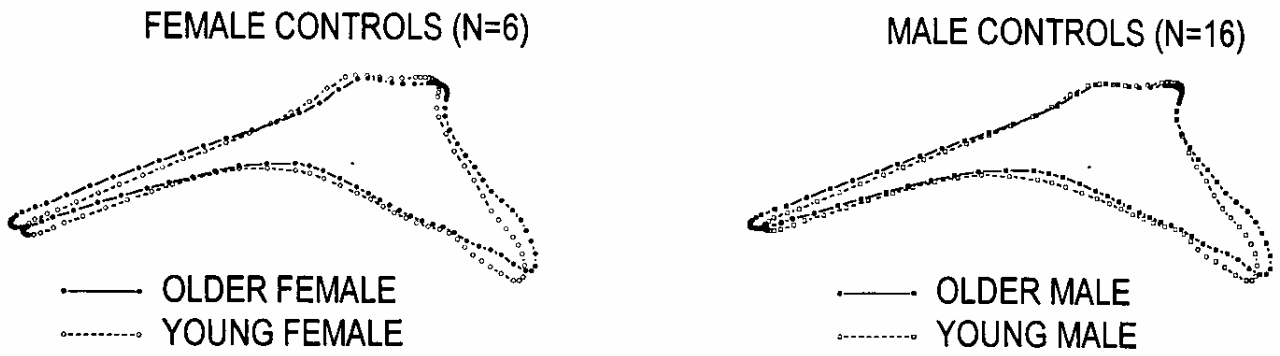

FIGURE 5 Computer-generated plots of the mean maxillary outline of the young controls superimposed on the older controls. The data have been standardized for size and orientation in two-dimensional space, so only shape differences are involved. The plots are superimposed on the centroid.

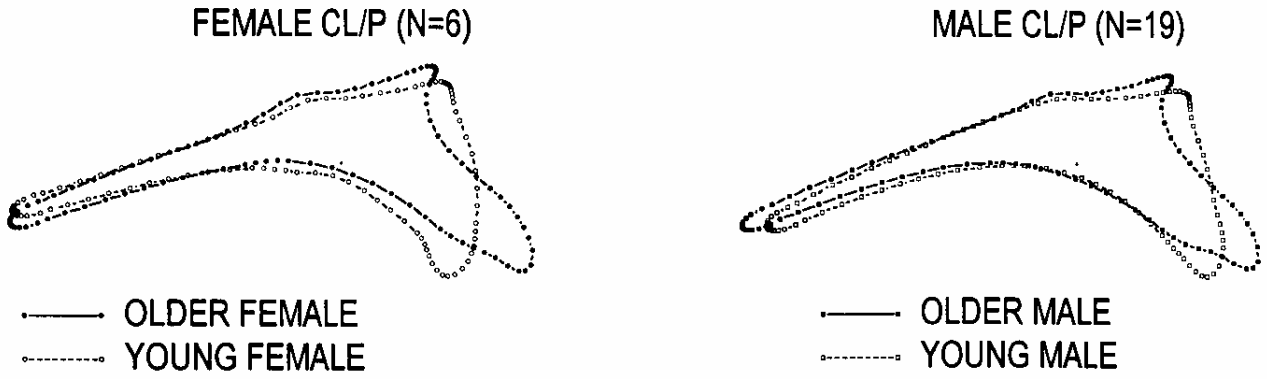

FIGURE 6 Computer-generated plots of the mean maxillary outline of the young CLP cases superimposed on the older CLP group. The data have been standardized for size and orientation in two-dimensional space, so only shape differences are involved. The plots are superimposed on the centroid.

columns on the right represent the generated points. Trisections are identified with asterisks.

Digitization

The maxillary tracings depicting the 48 points were then digitized using a digitizer (Calcomp, Inc., Scottsdale, AZ) accurate to 0.01 inch. Each tracing was superimposed on an origin (0,0), which was defined in the center of the digitizer by a set of crosshairs that were extended horizontally and vertically to the borders of the digitizer pad. The tracing was placed on the digitizer with PNS (point 1) on the origin (0,0) and the line from PNS to ANS (point 18), made coincident with the horizontal axis of the digitizer crosshairs.

Computation of EFFs

The digitized points were then submitted to a specially written routine (EFFA) (available from P.E.L.) that computes EFFs. These EFFs are close analogs of the bounded maxillary outline as judged by the residual or difference between the observed points and the predicted points (expected fit) generated by the Fourier function. Using 24 harmonics yielded a mean residual of 0.11 ± 0.02 mm, n = 50, which was deemed to be a satisfactory fit because these values are below the tracing, point location, and digitizing errors (Lestrel, 1980, 1982, 1989a). Each predicted maxillary outline was subsequently standardized for size by scaling the bounded area to a constant 10,000 mm^2. To correct for positioning, each outline was rotated so that the major axis of the first or principal ellipse of the EFF was made parallel to the x-axis to ensure a common orientation. Neither of these procedures, size standardization and positional orientation, can be precisely determined without the computation of EFFs.

The fit for an individual maxilla is shown as a stepwise procedure in Figure 3. With 12 harmonics, the residual fit averaged over the whole outline was 0.300 mm. With 24 harmonics, the residual value dropped to 0.127 mm. This value is below the errors associated with the tracing, location of points, and digitizing procedures (see next section). Slight losses in fit are present at PNS, at ANS, and at the tip of the central incisor, due to the sharp changes in curvature in these regions.

Error Analysis

Any estimate of errors has to be tempered with the knowledge that certain errors are difficult, if not impossible, to quan-

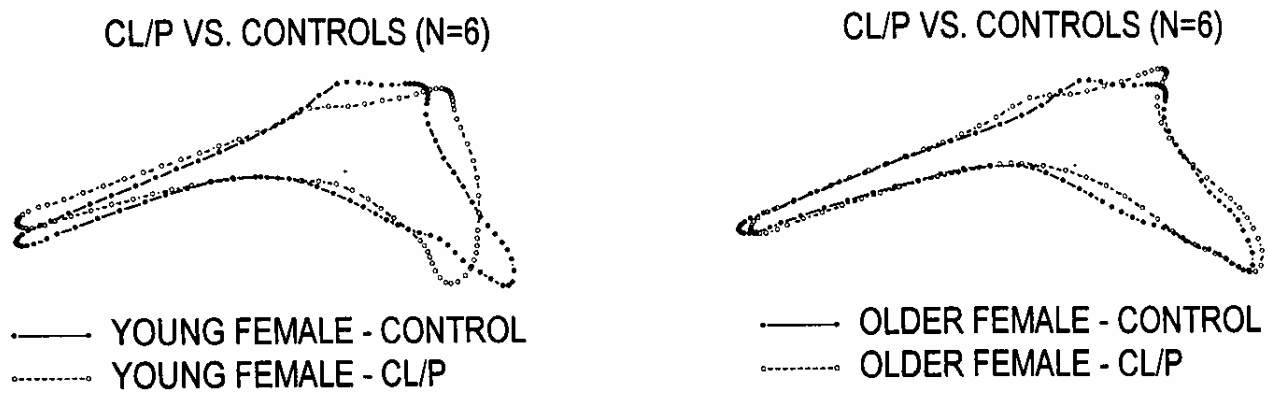

FIGURE 7 Computer-generated plots of the mean maxillary outline of the female controls superimposed on the female CLP cases. The data have been standardized for size and orientation in two-dimensional space, so only shape differences are involved. The plots are superimposed on the centroid.

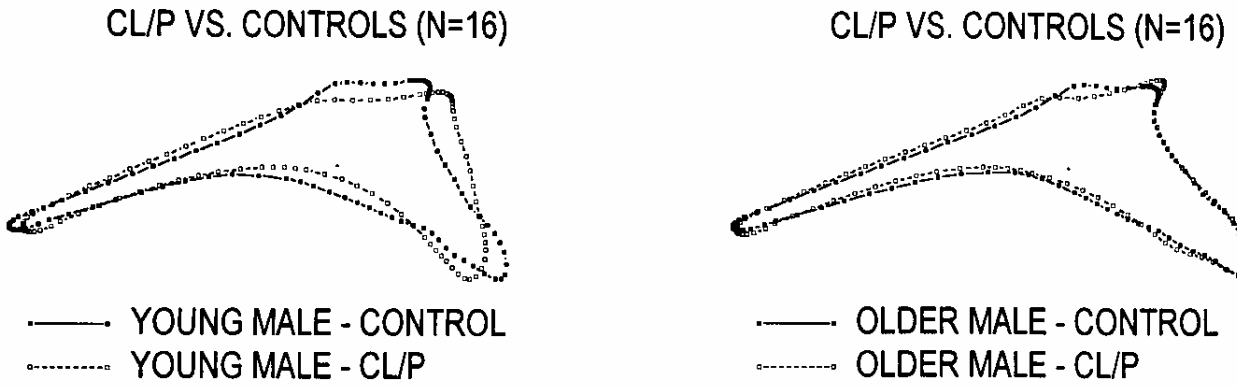

FIGURE 8 Computer-generated plots of the mean maxillary outline of the male controls superimposed on the male CLP cases. The data have been standardized for size and orientation in two-dimensional space, so only shape differences are involved. The plots are superimposed on the centroid.

tify, and these errors can add substantially to the error analysis. In this study, there are a number of such errors, which include head orientation, headfilm enlargement factors, and development quality. Nevertheless, the errors of the tracing, point location, and digitizing tasks can be evaluated.

An estimate of the reliability of the procedures involved in the maxilla study was computed from duplicate determinations of a random sample drawn from the maxilla control cases (n = 10). The error computation was based on the mean of the eight distances from the centroid to the maxilla boundary as calculated from the EFFs. The total error was based on the sum of the tracing of the maxilla outline, the placement of points, and the digitizing task. One investigator traced the maxilla outline and located the points twice on two different occasions and digitized the first one of these two data sets. The second data set was then independently digitized twice more by two different investigators. The total error (composed of tracing, point location, and digitizing) was estimated at 1.14 ± 0.80 mm. The error due solely to digitizing was calculated as 0.14 ± 0.09 mm. This indicates that the tracing and point location tasks in this study account for about 88% of the total error and that the digitizing accounts for about 12% of the total error.

Statistical Procedures

The statistical design consisted of testing for statistically significant differences in age (young and older groups), sex (males and females), and type (CLP and controls). Utilizing the standardized-for-size EFF curve fits, a set of distances from the centroid of each maxilla was computed. These eight distances were chosen to reflect the major structural aspects of the maxillary outline. Clearly, their choice contains a subjective element, and others could have been chosen equally as well. In addition to these eight distances, their x and y components were also calculated, yielding a set of 24 variables for subsequent analysis (Fig. 4; Table 2). (The justification for including the x and y components is that a major change in shape may be in the direction of a component and not along the distance itself.) Prior to the application of a three-way multivariate analysis of variance (MANOVA) to test the above contrasts, a correlation matrix was computed. The purpose of the correlation matrix was to reduce the large number of variables by removing variables that displayed high correlations, because such variables do not add much information. This was carried out by examining the pairwise correlations and removing one variable of each pair that displayed values equal to or greater than .70.

Results

The longitudinal data consisted of two time points, one at a young age, after lip surgery and the initialization of palatal surgery, and the other older group well after the conclusion of surgery. All data were standardized for size and positional orientation as described earlier. The following figures display the shape changes that occurred with growth and treatment in both the CLP and control groups. Figure 5 shows two sets of com-

TABLE 3 Means and Standard Deviations*

	D1	*D2*	*D3*	*D4*	*D5*	*D6*	*D7*	*D8*
Young groups								
CLP	175.66 ± 16.85	47.52 ± 5.32	78.59 ± 10.52	70.98 ± 13.10	85.47 ± 10.03	101.65 ± 11.39	66.29 ± 12.00	32.27 ± 15.91
Control	182.19 ± 15.79	54.24 ± 3.02	72.70 ± 4.21	55.95 ± 6.17	78.90 ± 8.00	114.89 ± 4.54	67.76 ± 6.74	21.55 ± 6.64
Older groups								
CLP	186.19 ± 16.89	50.77 ± 5.83	80.20 ± 8.77	56.25 ± 11.28	79.34 ± 6.25	119.50 ± 6.48	65.19 ± 8.16	37.20 ± 17.16
Control	187.45 ± 16.49	54.11 ± 2.15	71.12 ± 3.42	57.07 ± 4.69	77.07 ± 4.67	118.59 ± 3.84	64.18 ± 5.57	18.75 ± 7.20

* Mean and SD values for the CLP and control groups for the eight distances or vectors, D1 through D8, from the centroid to the maxillary outline. These are relative values, not actual, because they are based on size-standardized data (see text).

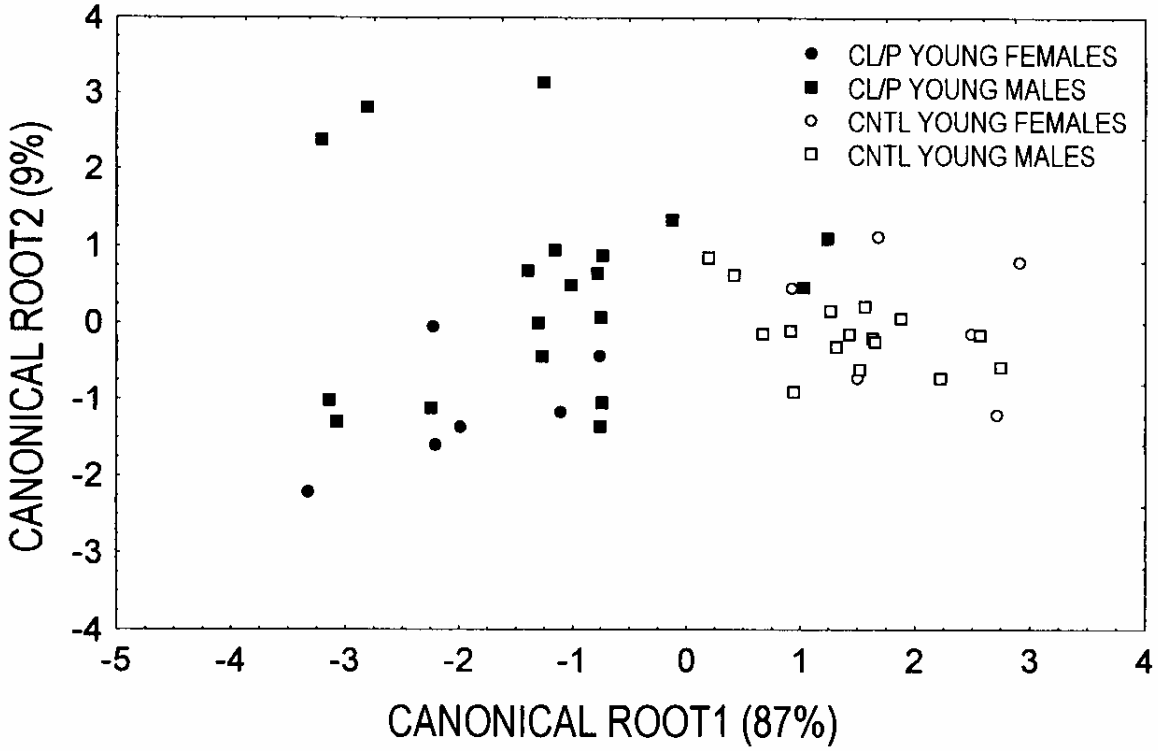

FIGURE 9 Canonical axes plot derived from discriminant function analysis. The CLP and control samples (broken down by sex) are shown here for both young groups.

puter-generated plots of the control maxilla outline. On the left is the young female age group superimposed on the centroid of the older female age group. On the right is the young male age group superimposed on the centroid of the older male age group. Figure 6 displays a similar comparison for the CLP female and male age groups. On the left are the young and older female CLP groups, and on the right are the young and older male CLP groups.

Of perhaps more clinical interest is the comparison of the CLP groups with their respective control counterparts. Figure 7 displays two computer-generated plots of the mean CLP and control maxillary outlines. On the left is the superimposition of the young female CLP group on the young female control group. On the right is the superimposition of the older female CLP group on the older female control group. Figure 8 shows a similar comparison for the males. On the left is the superimposition of the young male CLP group on the young male control group. On the right is the superimposition of the older male CLP group on the older male control group.

TABLE 4 Three-way MANOVA†

Contrast	*Wilks' Lambda*	*Rao's R*
Type***	.241	8.382
Sex	.833	0.533
Age***	.147	15.416

* $p < .05$; ** $p < .01$; *** $p < .001$.

† Three-way MANOVA table displaying the two between-group contrasts, type (CLP versus controls) and sex (females versus males), and the one within-group or repeated measure, age (young versus older).

Table 3 displays the means and SDs of the eight distances or vectors from the centroid, D1 through D8, used to characterize the maxillary outline. These distance values are relative values, not actual, because they are based on shape data. They are computed from the size-standardized EFFs. Thus, they are based on the bounded area of each maxillary outline after it has been scaled to a constant area to correct for size.

To statistically analyze whether the size-standardized visual differences displayed in Figures 5 through 8 are significant, a three-way MANOVA was utilized.[1] The data initially consisted of 24 variables, eight distances, and their x and y components (Fig. 4; Table 2). A correlation matrix confirmed the presence of moderate to high correlations. One variable of each pair displaying an $r \geq .70$ was therefore removed. This reduced the data set by 50% to 12 variables. The variables retained for further analysis were D1, D2, D3, D4, D6, D7, D8, Y1, Y4, Y5, Y6, and Y8. No x components were included. No obvious reason for the lack of x components is readily apparent; most likely, it is a consequence of sampling. Utilizing these 12 variables, a three-way MANOVA was computed. The "between contrasts" were sex and type, while age was the "within contrast" (repeated measure). Table 4 displays the MANOVA results with statistically significant differences between CLP and controls, and it documents the presence of an age effect. Sex differences, by contrast, were insignificant. As females super-

[1] Statistica, Version 5.1, Statsoft, Inc., Tulsa, OK. Some of the statistical results were also independently checked with SAS Institute Inc., Cary, NC.

TABLE 5 Univariate *F* Tests; Main Contrast (Age): Young Versus Older*

Variable	*Among-Mean-Square*	*Within-Mean-Square*	*F Ratio*	*Probability*
D1	666.952	82.554	8.079	$p < .006$
D2	41.944	11.005	3.811	ns
D3	6.271	41.179	0.152	ns
D4	866.784	25.899	33.468	$p < .001$
D6	2604.296	34.278	75.977	$p < .001$
D7	29.055	46.352	0.627	ns
D8	5.062	71.779	0.071	ns
Y1	15.473	26.526	0.583	ns
Y4	752.824	37.167	20.255	$p < .001$
Y6	4309.614	62.040	69.466	$p < .001$
Y7	398.172	22.894	17.392	$p < .001$
Y8	148.662	19.734	7.533	$p < .009$

* Degrees of freedom 1, 43. Distances D1, D4, and D6, as well as the y components Y4, Y6, Y7, and Y8, are statistically significant.

TABLE 6 Univariate *F* Tests; Main Contrast (Type): CLP Versus Controls*

Variable	*Among-Mean-Square*	*Within-Mean-Square*	*F Ratio*	*Probability*
D1	300.197	482.492	0.622	ns
D2	535.611	28.634	8.706	$p < .001$
D3	1065.719	77.033	3.835	$p < .001$
D4	860.363	169.692	5.070	$p < .030$
D6	896.493	67.090	13.363	$p < .001$
D7	0.005	101.695	0.001	ns
D8	5603.256	259.483	21.594	$p < .001$
Y1	82.671	61.278	1.349	ns
Y4	37.252	31.950	1.166	ns
Y6	184.704	119.698	1.543	ns
Y7	2.882	61.843	0.047	ns
Y8	144.924	52.860	2.742	ns

* Degrees of freedom 1, 43. Distances D2, D3, D4, and D6 as well as the y component Y8 are statistically significant.

imposed very closely on males for both the CLP and control groups, these figures were excluded here. These results were not unexpected because sexual dimorphism is largely influenced by size differences.

Table 5 depicts the univariate *F* tests for the age comparison between the younger and older age groups. Variables D1, D4, D6, Y4, Y6, Y7, and Y8 were statistically significant. Table 6 shows the univariate *F* tests for the type comparison between CLP and controls. Only variables D2, D3, D4, D6, and D8 were now statistically significant. These variables were generally in accord with the visual representation (Figs. 7 and 8).

Another multivariate approach was employed to see if these differences between the CLP and control groups could be numerically and visually described. This procedure is known as discriminant function analysis (Lubischew, 1962; Klecka, 1980). A unique linear function (discriminant) was computed for each maxillary outline, and the results were plotted on a set of canonical axes. A point graphed on such a canonical axis plot represents the summation of all the retained variables (those not removed) in the stepwise discriminant function analysis. Such a plot facilitates the reduction of higher dimensionality data to two-dimensional graphical representation. This procedure was carried out independently for the young and older groups.

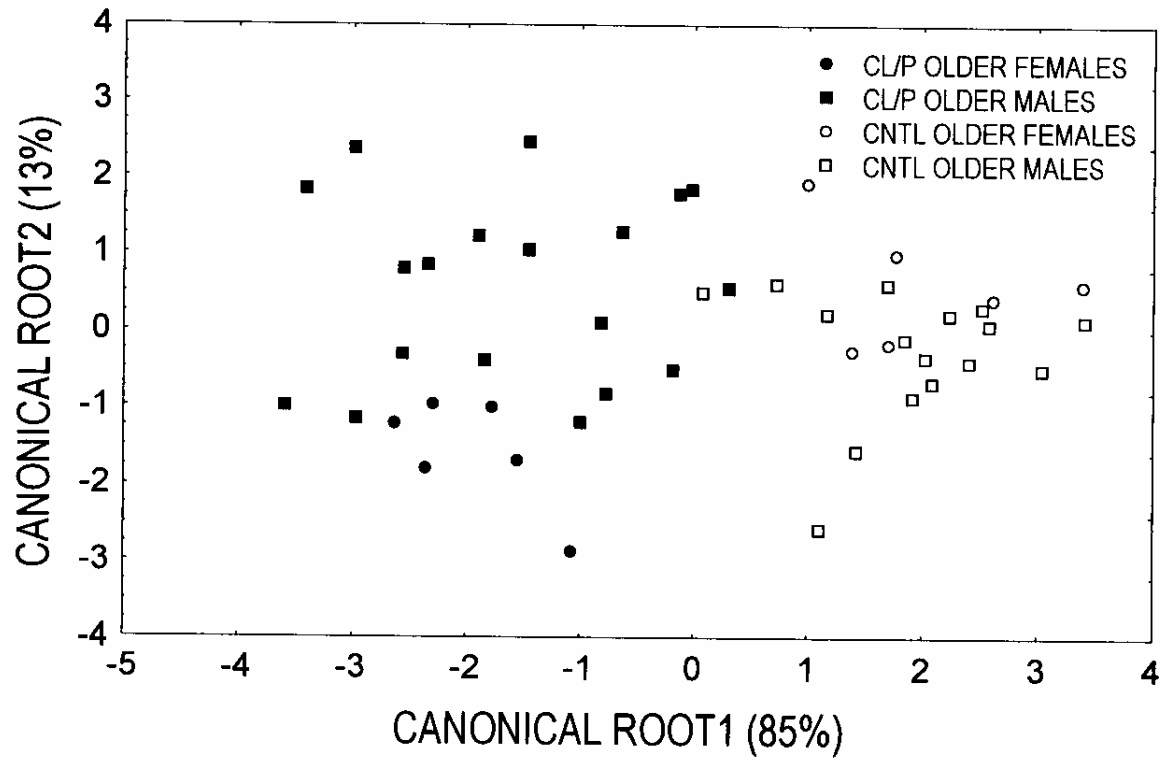

FIGURE 10 Canonical axes plot derived from discriminant function analysis. The CLP and control samples (broken down by sex) are shown here for both older groups.

TABLE 7 Stepwise Discriminant Analysis; Mahalanobis D^2 Values†

	CLP Females	*CLP Males*	*Control Females*	*Control Males*
CLP females	—	3.34	19.18***	13.73***
CLP males	5.32	—	12.44***	8.28***
Control females	22.11***	14.40***	—	1.56
Control males	18.21***	14.07***	1.50	—

* $p < .05$; ** $p < .01$; *** $p < .001$.

† Shown here are the distances between group centroids. Statistically significant distances are present between the CLP and control groups but not within the young and older groups (see text).

Figure 9 displays the young CLP female and male groups as well as the control female and male samples distributed along the first two canonical axes. Canonical axis 1 explains 87% of the variability in these data and clearly distinguishes the CLP groups (female and male) from the control groups (female and male). Moreover, the differences between the CLP and control groups are significant. Figure 10 illustrates the same comparison but for the older age groups. Canonical axis 1 explains 85% of the variability, and again, the differences between the older CLP and control age groups are statistically significant.

Table 7 summarizes one aspect of the stepwise discriminant function analysis results. Separate tests were carried out for the young and older age groups. The values depicted here are the distances between group centroids for the four samples: female and male CLP groups and female and male control samples. These distances are Mahalanobis D^2 values (with their associated significance values). The values above the diagonal refer to the young age groups, and the values below the diagonal are for the older age groups.

Discussion

While there is little question that the CLP cases were satisfactorily treated, the results here suggest that residual differences remain. Since differences in size were largely controlled for by scaling each maxillary outline to a constant area, these are differences solely in shape. Figures 7 and 8 illustrate these shape differences between the CLP and controls. Figures 9 and 10 also display these differences using the multivariate procedure of discriminant function analysis. The pattern is similar whether viewed at a young or older age and whether males or females are involved. With respect to the differences between the CLP subjects and controls, the major difference consists largely of a posterior repositioning of the nasal crest aspect. Other, more moderate differences are also present at ANS and the central incisor tip, but these are certainly within orthodontic and orthopedic clinical norms.

While these results are suggestive, it is cautioned that the sample sizes are marginal, especially the CLP females (n = 6). Moreover, only one aspect of the maxilla, the bounded outline as seen on the lateral radiograph, was analyzed. Since these data are longitudinal in the sense that young and older ages were compared, it would also be useful to analyze the complete data set (Fig. 1). Future studies should be conducted with larger sample sizes and with a more exhaustive analysis (i.e., one not limited to two dimensions) of the morphology of the maxillary complex.

Conclusions

This study has focused on two central issues. The first one was the need for unambiguous procedures to measure residual shape changes in the CLP maxilla, prior to the initiation, during, and after the conclusion of treatment, as an approach to test the efficacy of treatment outcomes. Concomitantly, the second one was the need for a numerical method that could precisely describe such shape changes in irregular morphologies such as the maxilla. While other techniques, such as finite elements, thin-plate splines, and EDMA, may generate comparable numerical results and provide precise statistical results, they tend to be more difficult to readily comprehend. Moreover, they rarely allow for a clear visual assessment of the results. Elliptical Fourier functions, by contrast, are particularly suitable for visually depicting these morphological shape changes in a way that may be deemed clinically meaningful.

The findings presented here were not anticipated at the initiation of the study. The CLP maxillary shape differences, consisting of a repositioning of the nasal crest aspect, could not have been identified with the CMA. They required a procedure that facilitated global as well as local analysis. While the surgery and the orthopedic and orthodontic procedures can be considered satisfactory, consistent shape differences after treatment and maturation remained in the CLP maxilla. However, to suggest that these CLP maxillary differences are important is perhaps premature and will require follow-up studies. Nevertheless, studies such as this one may lead to the development of refined treatment procedures so that future CLP patients may more closely resemble normals in every respect. That, after all, is the goal of all treatment outcomes.

Acknowledgments. We are indebted to Dr. Kornmiller, Department of Orthodontics, Oregon Health Sciences University, Portland (OR), for granting access to the cephalometric radiographs of the Oregon Longitudinal Twin Study. Supported by the Health Foundation of South Florida, Inc. We also would like to acknowledge the programming effort and technical assistance of Charles Wolfe of Wolfe Software Associates.

References

Berkowitz S. Stereophotogrammetric analysis of casts of normal and abnormal palates. *Am J Orthod* 1971;60:1–18.

Berkowitz S. *Cleft Lip and Palate.* San Diego: Singular Press; 1997.

Berkowitz S, Krischer J, Pruzansky S. Quantitative analysis of cleft palate casts. *Cleft Palate J* 1974;11:134–160.

Berkowitz S, Pruzansky S. Stereophotogrammetry of serial casts of cleft palate. *Angle Orthod* 1968;38:136–149.

Bishara SE, Martinez RS, Patron VH. Dentofacial relationships in persons with unoperated clefts: comparisons between three cleft types. *Am J Orthod* 1985;88:481–507.

Blum H. A transformation for extracting new descriptors of shape. In: Wathen-Dunn W, ed. *Models for the Perception of Speech and Visual Form.* Cambridge: MIT Press; 1967.

Blum H. Biological shape and visual science. *J Theor Biol* 1973;38:205–287.

Bookstein FL. *The Measurement of Biological Shape and Shape Change. Lecture Notes in Biomathematics.* New York: Springer-Verlag; 1978;24:1–191.

Bookstein FL. On the cephalometrics of skeletal change. *Am J Orthod* 1982;82: 177–182.

Bookstein FL. *Morphometric Tools for Landmark Data.* Cambridge: Cambridge University Press; 1991.

Cheverud JM, Richtsmeier JT. Finite-element scaling applied to sexual dimorphism in rhesus macaque (*Macaca mulatta*) facial growth. *Syst Zool* 1986;35:381–399.

Delfino VP, Colonna M, Vacca E, Potente F, Introna J. Computer-aided skull/face superimposition. *Am J Forensic Med Pathol* 1986;7:201–212.

Diaz G, Quacci D, Dell'Orbo C. Recognition of cell surface modulation by elliptic Fourier analysis. *Comput Methods Programs Biomed* 1990;31:57–62.

Ferson S, Rohlf FJ, Koehn RK. Measuring shape variation of two-dimensional outlines. *Syst Zool* 1985;43:59–68.

Heidbuchel KLWM, Kuijpers-Jagtman AM. Maxillary and mandibular dental-arch dimensions and occlusion in bilateral cleft lip and palate patients from 3 to 17 years of age. *Cleft Palate J* 1997;34:21–26.

Inoue M. Fourier analysis of the forehead shape of skull and sex determination by use of the computer. *Forensic Sci Int* 1990;47:101–112.

Johnson DR. Shape of vertebrae—an application of a generalized method. In: Dixon AD, Sarnat BG, eds. *Normal and Abnormal Bone Growth: Basic and Clincial Research.* New York: Alan R. Liss; 1985.

Jonsson G, Thilander B. Occlusion, arch dimensions, and craniofacial morphology after palatal surgery in a group of children with clefts in the secondary palate. *Am J Orthod* 1976;76:243–255.

Kilpeläinen PVJ, Laine-Alava MT, Lammi S. Palatal morphology and type of clefting. *Cleft Palate J* 1996;33:477–482.

Klecka WR. *Discriminant Analysis.* Quat. Appl. Soc. Sci. Ser. 19. Beverly Hills, CA: Sage; 1980.

Kuhl FP, Giardina CR. Elliptic Fourier features of a closed contour. *Comput Graphics Imaging Proc* 1982;18:236–258.

Lele S. Euclidean distance matrix analysis (EDMA): estimation of mean form and mean form difference. *Math Geol* 1993;25:573–602.

Lele S, Richtsmeier JT. Euclidean distance matrix analysis: a coordinate free approach for comparing biological shapes using landmark data. *Am J Phys Anthropol* 1991;86:415–427.

Lele S, Richtsmeier JT. On comparing biological shapes: detection of influential landmarks. *Am J Phys Anthropol* 1992;87:49–66.

Lestrel PE. Some problems in the assessment of morphological size and shape differences. *Yearb Phys Anthropol* 1974;18:140–162.

Lestrel PE. A quantitative approach to skeletal morphology: Fourier analysis. *SPIE* 1980;166:80–93.

Lestrel PE. A Fourier analytic procedure to describe complex morphologica shapes. In: Dixon AD, Sarnat BG, eds. *Factors and Mechanisms Influencing Bone Growth.* New York: Alan R. Liss; 1982.

Lestrel PE. Method for analyzing complex two-dimensional forms: elliptica Fourier functions. *Am J Hum Biol* 1989a;1:149–164.

Lestrel PE. Some approaches toward the mathematical modeling of the craniofacial complex. *J Craniofac Genet Dev Biol* 1989b;9:77–91.

Lestrel PE. Introduction and overview of Fourier descriptors. In: Lestrel PE ed. *Fourier Descriptors and Their Applications in Biology.* Cambridge Cambridge University Press; 1997a.

Lestrel PE. Morphometrics of craniofacial form. In: Dixon AD, Hoyte DAN Rönning O, eds. *Fundamentals of Craniofacial Growth.* Boca Raton, FL CRC Press; 1997b.

Lestrel PE, Engstrom C, Chaconas SJ, Bodt A. A longitudinal study of the human nasal bone in *Norma lateralis*: size and shape considerations. In: Dixon AD, Sarnat BG, Hoyle DAN, eds. *Fundamentals of Bone Growth. Methodology and Applications.* Boca Raton, FL: CRC Press; 1991.

Lestrel PE, Kerr WJS. Quantification of functional regulator therapy using elliptical Fourier functions. *Eur J Orthod* 1993;15:481–491.

Lohmann GP. Eigenshape analysis of microfossils: a general morphometric procedure for describing changes in shape. *Math Geol* 1983;15:659–672.

Lohmann GP, Schweitzer PN. On eigenshape analysis. In: Rohlf FJ, Bookstein FL, eds. *Proceedings of the Michigan Morphometric Workshop.* University of Michigan Museum of Zoology Special Publ. 2; 1990.

Lubischew AA. On the use of discriminant functions in taxonomy. *Biometrics* 1962;18:455–477.

Mølsted K, Dahl E. Asymmetry of the palate in children with complete unilateral cleft lip and palate. *Cleft Palate J* 1990;27:184–192.

Ray TS. Application of eigenshape analysis to second order leaf shape ontogeny in *Syngonium podophyllum* (Araceae). In: Rohlf FJ, Bookstein FL, eds. *Proceedings of the Michigan Morphometric Workshop.* University of Michigan Museum of Zoology Special Publ. 2; 1990.

Read DW. From multivariate to qualitative measurement: representation of shape. *Hum Evol* 1990;5:417–429.

Read DW, Lestrel PE. A comment upon the uses of homologous-point measures in systematics: a reply to Bookstein et al. *Syst Zool* 1986;33:241–253.

Richtsmeier JT. Cranial growth in Apert's syndrome as measured by finite element scaling analysis. *Acta Anat* 1988;133:50–56.

Rohlf FJ, Archie JW. A comparison of Fourier methods for the description of wing shape in mosquitos (Diptera: Culicidae). *Syst Zool* 1984;33:302–317.

Straney DO. Median axis methods in morphometrics. In: Rohlf FJ, Bookstein FL, eds. *Proceedings of the Michigan Morphometric Workshop.* University of Michigan Museum of Zoology Special Publ. 2; 1990.